Electronic Supplementary Material (ESI) for Journal of Materials Chemistry C.

Supporting Information for

Placing a crown on Dy(III) – a dual property Ln(III) crown ether complex displaying optical properties and SMM behaviour.

Emma L. Gavey,[a] Majeda Al Hareri,[a] Jeffery Regier,[a] Luis D. Carlos[d], Rute A.S. Ferreira,[d] Fereidoon S. Razavi[b] Jeremy M. Rawson,[c] and Melanie Pilkington*[a]

[a] Department of Chemistry, Brock University
500 Glenridge Avenue
St Catharines, ON
Canada. L2S 3A1
Tel: +1 (905) 688 5550; Ext. 3403
E-mail: mpilkington@brocku.ca

[b] Department of Physics, Brock University
500 Glenridge Avenue
St Catharines, ON
Canada. L2S 3A1

[c] Department of Chemistry and Biochemistry
University of Windsor
401 Sunset Avenue, Windsor
ON, Canada. N9B 3P4

[d] Department of Physics and CICECO Institute of Materials,
University of Aveiro, 3810-193, Portugal.

Table of Contents

S-1 Crystallographic data

1.1 Crystallographic data and structure refinement

Table 1.1 Crystal data and structure refinement for **(1)**, **(2)** and the yttrium(III) analogue of **(2)**.

	(1)	**(2)**	**$[Y(12C4)(H_2O)_5](ClO_4)_3 \cdot H_2O$**
Empirical formula	$C_{20}H_{50}Cl_3DyO_{27}$	$C_8H_{28}Cl_3O_{22}Dy$	$C_8H_{28}Cl_3O_{22}Y$
Formula weight	991.45	745.15	671.56
Temperature/K	150(2)	150(2)	150(2)
Crystal system	monoclinic	monoclinic	monoclinic
Space group	$P2_1/n$	$P2_1/c$	$P2_1/c$
***a*/Å**	15.8533(14)	13.1195(7)	13.139(1)
***b*/Å**	14.6908(14)	10.2129(6)	10.2303(7)
***c*/Å**	16.4867(15)	17.5681(10)	17.5916(14)
α/°	90	90	90
β/°	99.409(4)	93.941(2)	93.866(3)
γ/°	90	90	90
Volume/Å^3	3788.06	2348.4(2)	2359.2(3)
Z	1	4	4
ρ_{calc}mg/mm^3	1.735	2.164	1.8906
μ/mm^{-1}	2.278	3.618	2.936
F(000)	2004.0	1524.0	1358.8
Crystal size/mm^3	0.32 x 0.29 x 0.45	0.43 x 0.27 x 0.28	0.14 x 0.09 x 0.09
Independent reflections	7642	4806	5913
Goodness-of-fit on F^2	1.233	1.334	1.299
Final R indexes [I>=2σ (I)]	R_1 = 0.0460 wR_2 = 0.1394	R_1 = 0.0208 wR_2 = 0.0514	R_1 = 0.0417 wR_2 = 0.1421

1.2 Crystallographic data for (1)

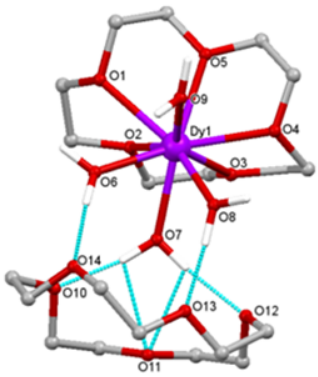

Fig. 1.2a View of the molecular structure of **(1)** showing the H-bonding interactions to the uncomplexed crown ether ligand as blue dashed lines.

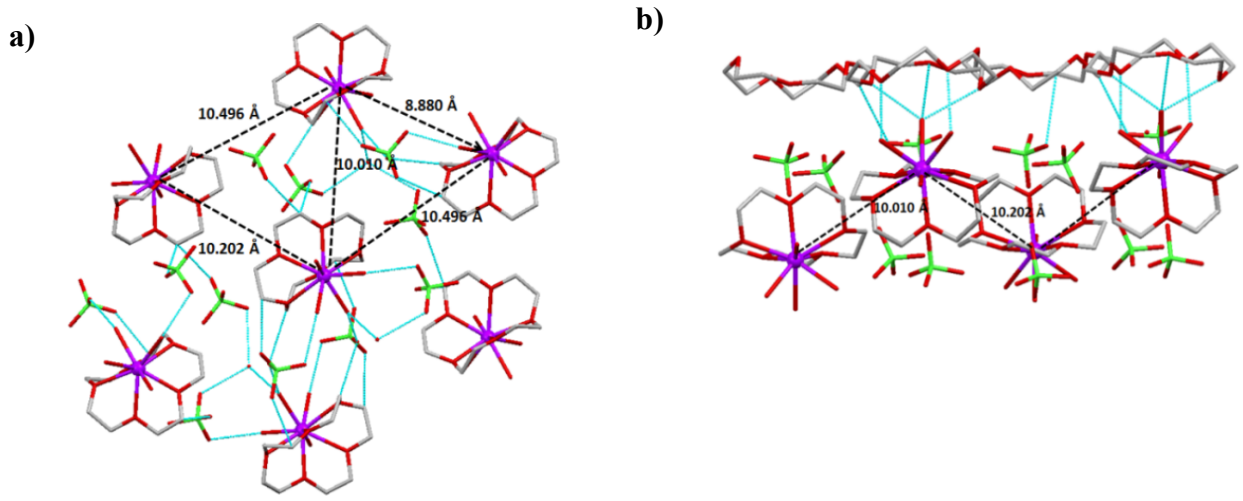

Fig 1.2b a) View of the crystal packing of **(1)** down the b(1/2a+1/2c) plane, showing $Dy^{II}\cdots Dy^{III}$ distances as black dashed lines; b) view of the crystal packing down the *b*-axis, showing the alternating layered arrangement of Dy^{III}-bound crown ether ligands, free H-bonded crowns, ClO_4^- counterions and lattice H_2O molecules. Hydrogen bonds are shown as dashed blue lines. Colour code: purple = Dy^{III}, grey = C, green = Cl, red = O.

Table 1.2 Selected bond lengths and angles for complex **(1)**.

Atom	*Atom*	*Length/Å*
Dy1	O1	2.513(6)
Dy1	O2	2.420(6)
Dy1	O3	2.495(5)
Dy1	O4	2.457(6)
Dy1	O5	2.446(6)
Dy1	O6	2.337(6)
Dy1	O7	2.386(6)
Dy1	O8	2.372(6)
Dy1	O9	2.344(5)

Atom	**Atom**	**Atom**	**Angle/°**
O2	Dy1	O1	62.74(19)
O3	Dy1	O1	118.23(19)
O3	Dy1	O2	62.79(18)
O4	Dy1	O1	129.5(2)
O4	Dy1	O2	121.6(2)
O4	Dy1	O3	64.66(19)
O5	Dy1	O1	65.2(2)
O5	Dy1	O2	87.0(2)
O5	Dy1	O3	85.2(2)
O5	Dy1	O4	65.0(2)
O6	Dy1	O1	66.8(2)
O6	Dy1	O2	90.2(2)
O6	Dy1	O3	138.1(2)
O6	Dy1	O4	147.8(2)
O6	Dy1	O5	127.1(2)
O7	Dy1	O1	117.2(2)
O7	Dy1	O2	74.0(2)
O7	Dy1	O3	71.7(2)
O7	Dy1	O4	111.2(2)
O7	Dy1	O5	154.93(18)
O7	Dy1	O6	70.3(2)

O8	Dy1	O1	141.5(2)
O8	Dy1	O2	142.2(2)
O8	Dy1	O3	100.0(2)
O8	Dy1	O4	70.0(2)
O8	Dy1	O5	126.9(2)
O8	Dy1	O6	81.9(2)
O8	Dy1	O7	68.5(2)
O9	Dy1	O1	79.3(2)
O9	Dy1	O2	141.8(2)
O9	Dy1	O3	143.0(2)
O9	Dy1	O4	79.0(2)
O9	Dy1	O5	72.68(19)
O9	Dy1	O6	77.9(2)
O9	Dy1	O7	132.13(19)
O9	Dy1	O8	72.5(2)
C1	O1	Dy1	120.2(5)
C10	O1	Dy1	114.6(5)
C2	O2	Dy1	115.3(4)
C3	O2	Dy1	121.0(5)
C4	O3	Dy1	122.8(5)
C5	O3	Dy1	121.5(4)
C6	O4	Dy1	114.7(5)
C7	O4	Dy1	118.2(5)
C8	O5	Dy1	122.5(5)
C9	O5	Dy1	120.6(5)

1.3 Crystallographic data for (2)

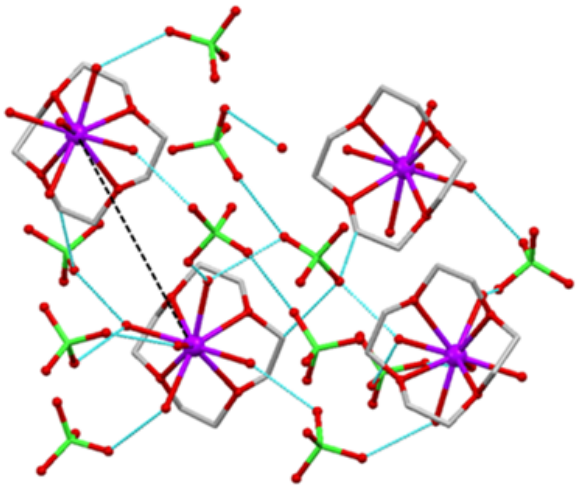

Fig 1.3 Crystal packing of **(2)**; view down the *b*-axis, showing H-bonds as blue dashed lines. Colour code: purple = Dy^{III}, grey = C, green = Cl, red = O. The shortest Dy···Dy distance of 8.875(5) Å is shown as a black dashed line.

Table 1.3. Selected bond lengths and angles for complex **(2)**.

Atom	*Atom*	*Length/Å*
Dy01	O1	2.4739(19)
Dy01	O2	2.515(2)
Dy01	O3	2.480(2)
Dy01	O4	2.551(2)
Dy01	O5	2.343(2)
Dy01	O6	2.317(2)
Dy01	O7	2.435(2)
Dy01	O8	2.378(2)
Dy01	O9	2.335(2)

Atom	**Atom**	**Atom**	**Angle/°**
O1	Dy01	O2	64.33(7)
O1	Dy01	O3	96.51(7)
O1	Dy01	O4	64.80(6)
O2	Dy01	O4	99.25(7)

O3	Dy01	O2	64.88(6)
O3	Dy01	O4	63.78(7)
O5	Dy01	O1	69.20(7)
O5	Dy01	O2	79.90(7)
O5	Dy01	O3	144.66(7)
O5	Dy01	O4	128.61(7)
O5	Dy01	O7	70.36(7)
O5	Dy01	O8	140.64(7)
O6	Dy01	O1	131.30(7)
O6	Dy01	O2	69.92(7)
O6	Dy01	O3	78.04(8)
O6	Dy01	O4	140.91(7)
O6	Dy01	O5	87.59(8)
O6	Dy01	O7	69.72(7)
O6	Dy01	O8	82.12(8)
O6	Dy01	O9	140.67(8)
O7	Dy01	O1	132.44(7)
O7	Dy01	O2	130.12(7)
O7	Dy01	O3	131.05(7)
O7	Dy01	O4	130.61(7)
O8	Dy01	O1	141.64(7)
O8	Dy01	O2	130.09(7)
O8	Dy01	O3	69.48(7)
O8	Dy01	O4	77.16(7)
O8	Dy01	O7	70.42(7)
O9	Dy01	O1	78.91(7)
O9	Dy01	O2	142.62(7)
O9	Dy01	O3	129.38(7)
O9	Dy01	O4	69.10(7)
O9	Dy01	O5	80.98(8)
O9	Dy01	O7	70.99(7)
O9	Dy01	O8	83.35(8)
C1	O1	Dy01	115.65(16)
C8	O1	Dy01	122.39(16)
C6	O2	Dy01	119.33(16)
C7	O2	Dy01	112.79(16)
C4	O3	Dy01	123.29(17)

C5	O3	Dy01	114.98(16)
C2	O4	Dy01	117.75(16)
C3	O4	Dy01	112.84(17)

1.4 Unit cell data for doped (2)

Table 1.4 Comparison of unit cell dimensions for **(2)**, the yttrium(III) analogue of **(2)**, and the doped sample of **(2)**.

	(2)	**$[Y(12C4)(H_2O)_5](ClO_4)_3 \cdot H_2O$**	**Doped (2)**
Crystal system	monoclinic	monoclinic	monoclinic
Space group	$P2_1/c$	$P2_1/c$	$P2_1/c$
***a*/Å**	13.1195(7)	13.139(1)	13.10
***b*/Å**	10.2129(6)	10.2303(7)	10.19
***c*/Å**	17.5681(10)	17.5916(14)	17.55
α/°	90	90	90
β/°	93.941(2)	93.866(3)	93.72
γ/°	90	90	90
Volume/Å^3	2348.4(2)	2359.2(3)	2342

1.5 SHAPE parameters[1]

Table **1.5** Shape measures of the 9-coordinate Dy^{III} coordination polyhedra in complexes **(1)** and **(2)**. The values in red indicate the closest polyhedron for each complex, according to the continuous shape measures. Complex **(1)** appears to adopt a muffin geometry, while complex **(2)** approximates a capped square anti-prism.

Polyhedron	**Dy^{III}_1**	**Dy^{III}_2**
EP-9	**35.20**	**36.27**
OPY-9	**24.16**	**23.10**
HBPY-9	**14.51**	**18.48**
JTC-9	**15.58**	**16.09**
JCCU-9	**7.51**	**7.30**
CCU-9	**6.38**	**6.22**
JCSAPR-9	**2.57**	**1.37**
CSAPR-9	**1.78**	**0.51**

JTCTPR-9	**3.69**	**2.69**
TCTPR-9	**2.59**	**1.49**
JTDIC-9	**10.68**	**12.72**
HH-9	**9.81**	**11.73**
MFF-9	**1.27**	**1.12**

Abbreviations: EP-9, Enneagon; OPY-9, Octagonal pyramid; HBPY-9, Heptagonal bipyramid; JTC-9, Johnson triangular cupola J3; JCCU-9, Capped cube J8; CCU-9, Spherical-relaxed capped cube; JCSAPR-9, Capped square antiprism J10; CSAPR-9, Spherical capped square antiprism; JTCTPR-9, Tricapped trigonal prism J51; TCTPR-9, Spherical tricapped trigonal prism; JTDIC-9, Tridiminished icosahedron J63; HH-9, Hula-hoop; MFF-9, Muffin.

Fig. 1.5 Coordination spheres of complexes **(1)** (left) and **(2)** (right). Colour code: grey = Dy^{III}, red = O, beige = idealized polyhedra.

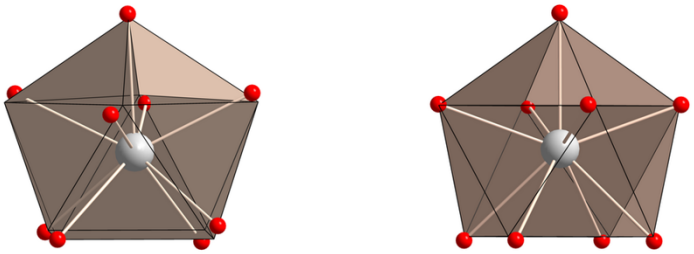

S-2 Magnetic data

Note: unless otherwise stated, solid lines are a guide for the eyes only.

Samples of **(1)** and **(2)** comprised multiple single crystals fixed in a gelatin capsule using apiezon grease. Multiple samples of both **(1)** and **(2)** were measured from different preparations to confirm reproducibility. Magnetic measurements were carried out on polycrystalline samples.

2.1 Dc data for (1)

Fig. 2.1a Plot of χT *vs*. temperature for **(1)** from 5 - 300 K, with an average value of χT above 100 K of 13.77 $cm^3 \cdot K \cdot mol^{-1}$.

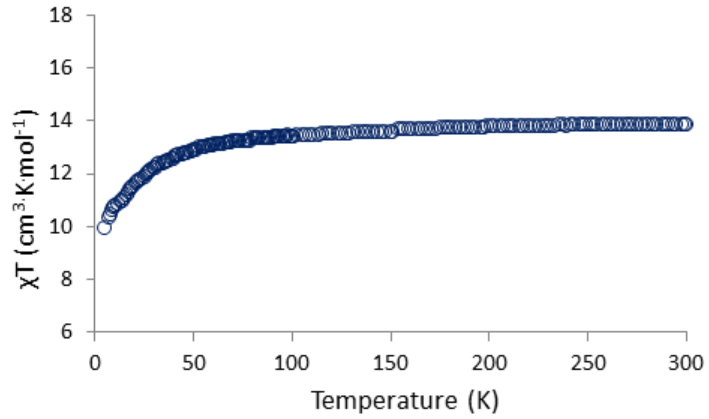

Fig. 2.1b Plot of 1/χ vs. temperature for **(1)** from 5 - 300 K. The black line is a best-fit to the Curie-Weiss law, giving C = 14.14 $cm^3 \cdot K \cdot mol^{-1}$ and a Weiss constant of -4.83 K.

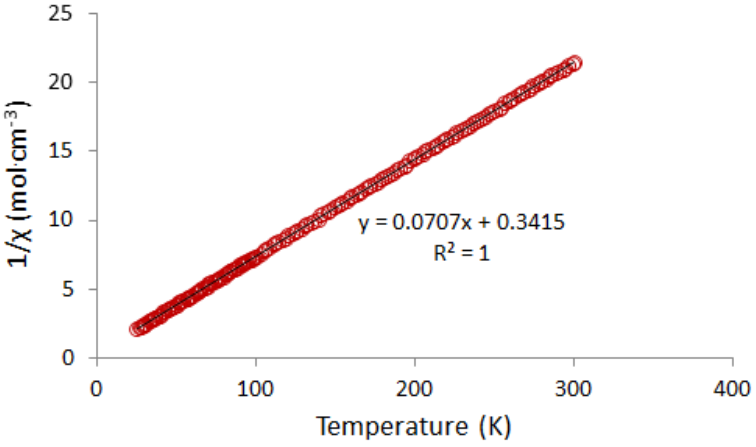

2.2 Dc data for (2)

Fig. 2.2a Plot of χT vs. temperature for **(2)** from 5 - 300 K, with an average value of χT above 100 K of 14.30 $cm^3 \cdot K \cdot mol^{-1}$.

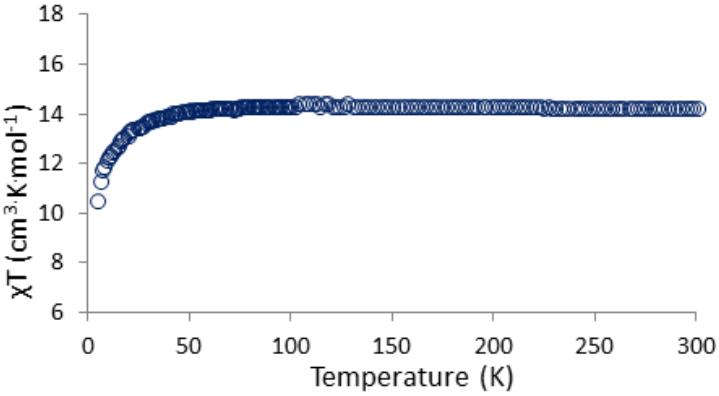

Fig. 2.2b Plot of $1/\chi$ vs. temperature for **(2)** from 5 - 300 K. The black line is a best fit to the Curie-Weiss law, giving $C = 14.70$ cm^3·K·mol^{-1} and a Weiss constant of -2.19 K.

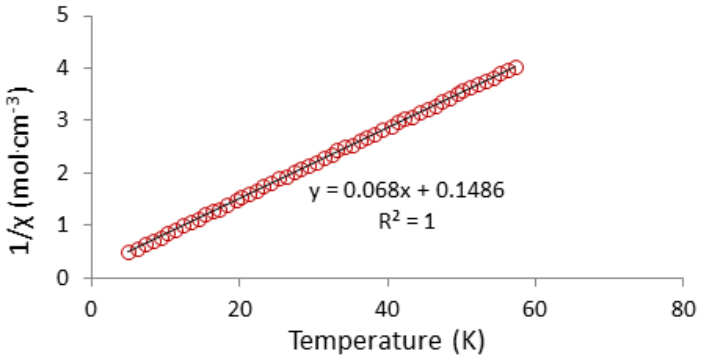

Fig. 2.2c Plot of magnetization versus field for **(2)** at 3 K.

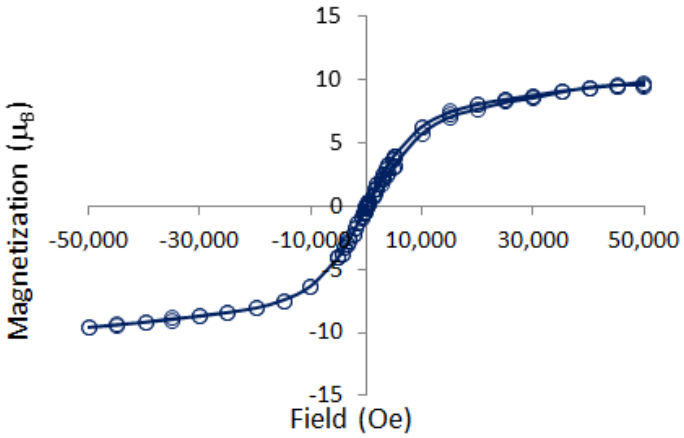

2.3 Additional ac data for (1) and (2)

Fig. 2.3a Plot of χ''_M vs. temperature for **(1)** in zero dc field, showing frequency dependent susceptibility but the absence of any maxima.

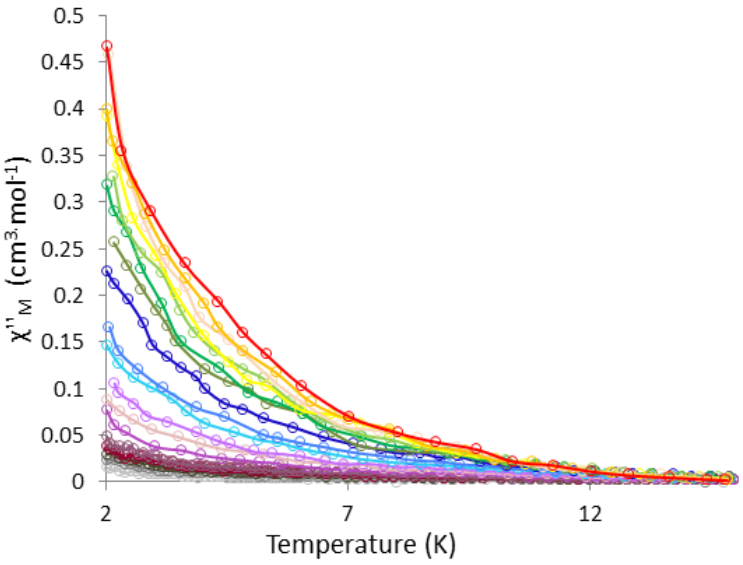

Fig. 2.3b Plot of χ'_M and χ''_M vs. temperature for **(1)** in 300 Oe applied dc field, below 15 K.

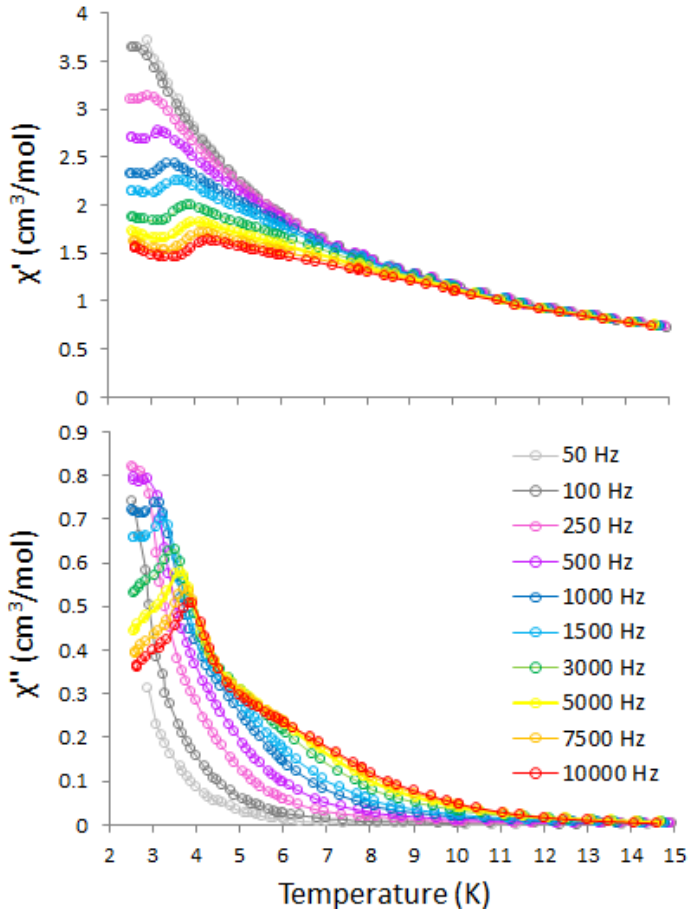

Fig. 2.3c Plot of χ''_M *vs.* χ'_M for **(2)** in 5000 Oe dc field, showing un-Debye-like behaviour.

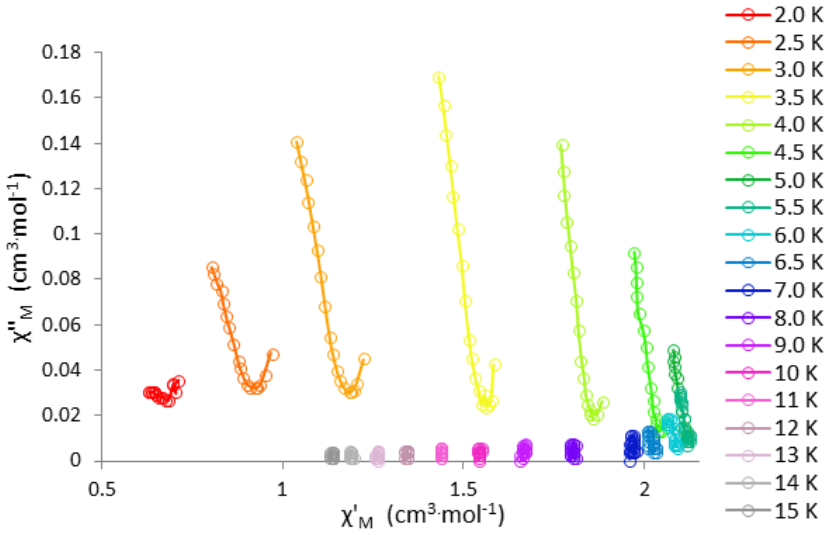

Fig. 2.3d Plot of $\delta(\chi''_M) / \delta(\frac{1}{T})$ versus frequency. A maximum occurs at 3000 Hz, corresponding to the point at which $\omega\tau = 1$. This gives an approximate value of $\tau = 0.3$ ms.

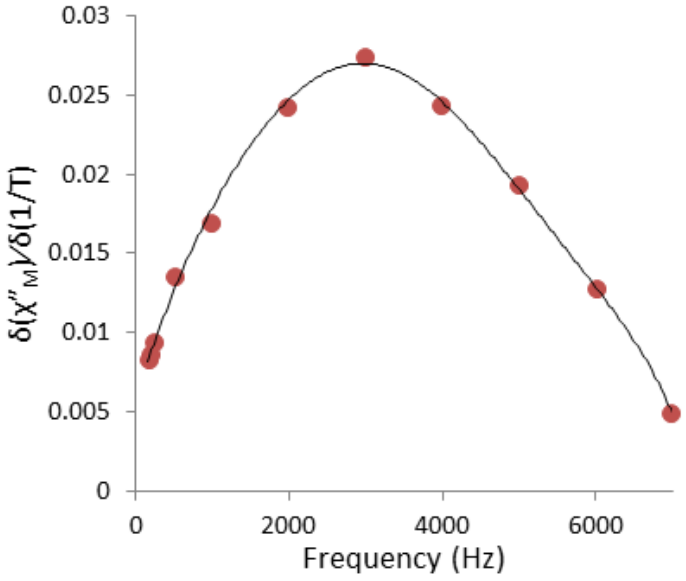

S-3 Equations[2]

The Cole-Cole model describes ac susceptibility as

$$\chi(\omega) = \chi_S + \frac{\chi_T - \chi_S}{1 + (i\omega\tau_c)^{1-\alpha}} \qquad \text{Eqn. 1}$$

where $\omega = 2\pi f$, χ_T is the isothermal susceptibility, χ_S is the adiabatic susceptibility, τ_c is the temperature-dependent relaxation time, and α is a measure of the dispersivity of relaxation times, with $\alpha = 0$ reflecting a single Debye-like relaxation time and $\alpha = 1$ reflecting an infinitely wide dispersion of τ_c values.

Dividing Eqn. 1 into its in-phase and out-of-phase components gives

$$\chi'(\omega) = \chi_S + \frac{(\chi_T - \chi_S)}{2}\left\{1 - \frac{sinh[(1-\alpha)ln(\omega\tau_c)]}{cosh[(1-\alpha)\ln(\omega\tau_c)] + cos\left[{}^{1}\!/_{2}(1-\alpha)\pi\right]}\right\} \qquad \text{Eqn. 2}$$

$$\chi''(\omega) = \frac{(\chi_T - \chi_S)}{2}\left\{1 - \frac{sin\left[{}^{1}\!/_{2}(1-\alpha)\pi\right]}{cosh[(1-\alpha)\ln(\omega\tau_c)] + cos\left[{}^{1}\!/_{2}(1-\alpha)\pi\right]}\right\} \qquad \text{Eqn. 3}$$

In the case of complex **(1)**, the susceptibility behaviour below 5 K is due to contributions from two distinct relaxation pathways. The relaxation in this temperature region can thus be described by the sum of two combined, modified Debye functions:

$$\chi(\omega) = \chi_{S1} + \frac{\chi_{T1} - \chi_{S1}}{1 + (i\omega\tau_{c1})^{1-\alpha 1}} + \chi_{S2} + \frac{\chi_{T2} - \chi_{S1}}{1 + (i\omega\tau_{c2})^{1-\alpha 2}} \qquad \text{Eqn. 4}$$

Dividing Eqn. 4 into its in-phase and out-of-phase components gives

$$\chi'(\omega) = \chi_S + (\chi_{T1} - \chi_S)\left\{\frac{1 + (\omega\tau_{c1})^{1-\alpha_1}\sin(\pi\alpha_1/2)}{1 + (\omega\tau_{c1})^{1-\alpha_1}\sin(\pi\alpha_1/2) + (\omega\tau_{c1})^{2-2\alpha_1}}\right\} \qquad \text{Eqn. 5}$$

$$+ (\chi_{T2} - \chi_S)\left\{\frac{1 + (\omega\tau_{c2})^{1-\alpha_2}\sin(\pi\alpha_2/2)}{1 + (\omega\tau_{c2})^{1-\alpha_2}\sin(\pi\alpha_2/2) + (\omega\tau_{c2})^{2-2\alpha_2}}\right\}$$

$$\chi''(\omega) = (\chi_{T1} - \chi_S)\left\{\frac{1 + (\omega\tau_{c1})^{1-\alpha_1}\cos(\pi\alpha_1/2)}{1 + (\omega\tau_{c1})^{1-\alpha_1}\sin(\pi\alpha_1/2) + (\omega\tau_{c1})^{2-2\alpha_1}}\right\} + (\chi_{T2} - \chi_S)\left\{\frac{1 + (\omega\tau_{c2})^{1-\alpha_2}\cos(\pi\alpha_2/2)}{1 + (\omega\tau_{c2})^{1-\alpha_2}\sin(\pi\alpha_2/2) + (\omega\tau_{c2})^{2-2\alpha_2}}\right\} \quad \text{Eqn. 6}$$

where $\chi_S = \chi_{S1} + \chi_{S2}$.

The Arrhenius equation, relating relaxation time τ_c to temperature T, is given by

$$\tau_c = \tau_0 e^{U_{eff}/k_B T} \quad \text{Eqn. 7}$$

where τ_0 is the tunneling rate and U_{eff} is the effective energy barrier.

S-4 Heat capacity data

Heat capacity measurements were conducted on a Quantum Design PPMS, between 2 and 50 K in zero applied field.

Fig. 4 Plots of heat capacity *vs*. temperature for **(1)** (top) and **(2)** (bottom) showing the lack of an abrupt λ-type transition, indicating the absence of a long-range magnetic ordering. The smooth increase in heat capacity upon warming is associated with the phonon (lattice) contribution to the specific heat.

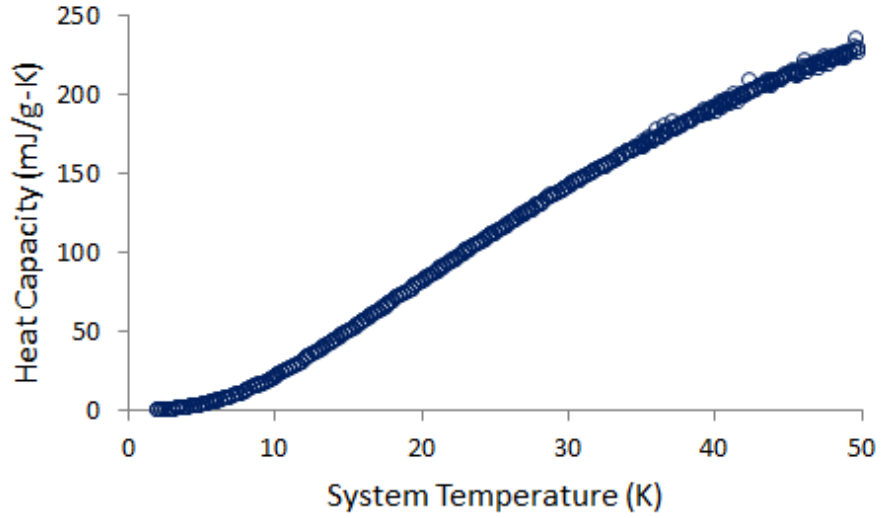

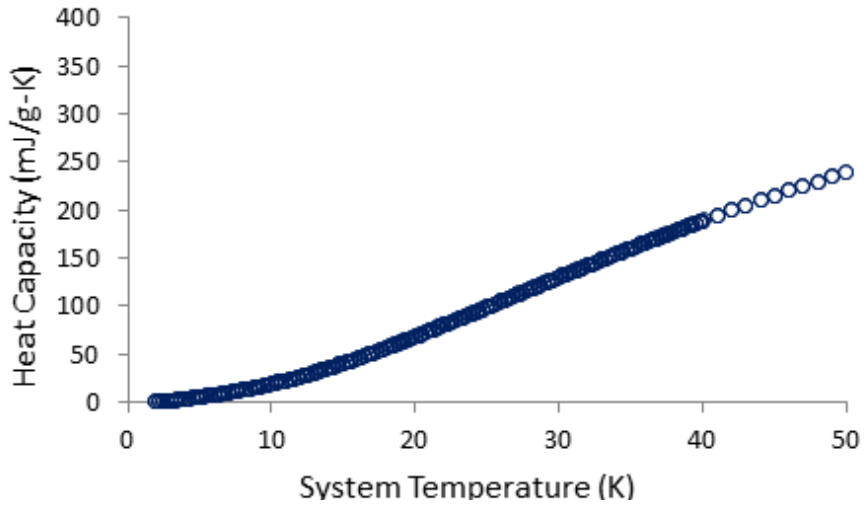

S-5 Quantum chemical calculations

5.1 Computational details

Ab initio calculations were performed using MOLCAS 7.8 quantum chemistry software.[3] The coordinates of the atoms were obtained by single crystal X-ray diffraction and were used without further geometry optimization. For all calculations, the multi-configurational CASSCF/RASSI-SO approach was used where the active space was chosen as the nine electrons in the seven 4*f*-orbitals of the dysprosium ion. Relativistic basis sets of the type ANO-RCC were chosen to

include the scalar relativistic terms where the dysprosium ions were treated at the VQZP level (9s8p6d4f3g2h), the coordinating oxygen atoms were treated at the VTZP level (4s3p2d1f) and all other atoms were treated at the VDZ level (3s2p for O and C, 4s3p for Cl, and 2s for H) for all models. The spin-free Eigenstates were calculated by the CASSCF method using the Douglas-Kroll-Hess Hamiltonian and then were mixed by following the RASSI-SO method to include spin-orbit coupling. The Dy^{III} ions were given the pseudo-spin $\tilde{S} = \frac{1}{2}$ for the calculations of the *g*-tensors of the eight Kramers′ doublets and the main magnetic axes. For the calculations of models **1A**, **1B**, **2A**, and **2B**, only the sextets were considered with 21 roots and no mixing from the quadruplets and doublets. However, in the calculations of the full models (**1C**, **2C**) mixing of the quadruplets were considered in the RASSI-SO module, where the sextets were given 21 roots and the quadruplets were given 128 roots.[4] No significant difference was observed between the eight Kramers′ doublets obtained with and without the inclusion of the quadruplets.

Three models for each complex were investigated in order to determine an accurate representation of the electronic structure of the complex within the crystal lattice. Complex **1** was modelled as just the immediate coordination sphere (**1A**), the asymmetric unit comprising two 15-crown-5s and water molecules (**1B**), and the full complex with one solvent water and three perchlorate anions that H-bond to the oxygen atoms of the water molecules that are directly coordinated to the Dy^{III} centre (**1C**).

Fig. 5.1 Three models calculated for complex **1**: **1A** (left), **1B** (centre) and **1C** (right).

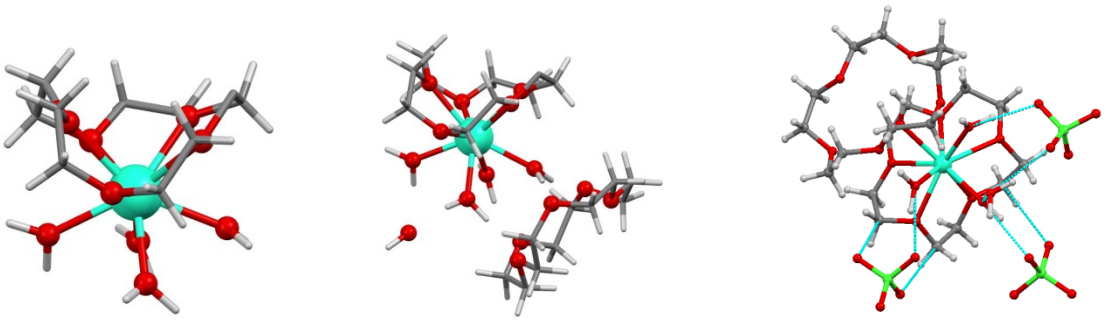

1A **1B** **1C**

For complex **(2)**, the first model was the immediate coordination sphere (**2A**). The second model (**2B**) includes the one solvent water and seven perchlorate anions that are H-bonded to the water molecules directly bound to the Dy^{III} center and the third model (**2C**) includes the three perchlorate anions in addition to the coordinated 12-crown-4 ligands and water molecule of the asymmetric unit.

Fig. **5.2** Three models calculated for complex **(2)**.

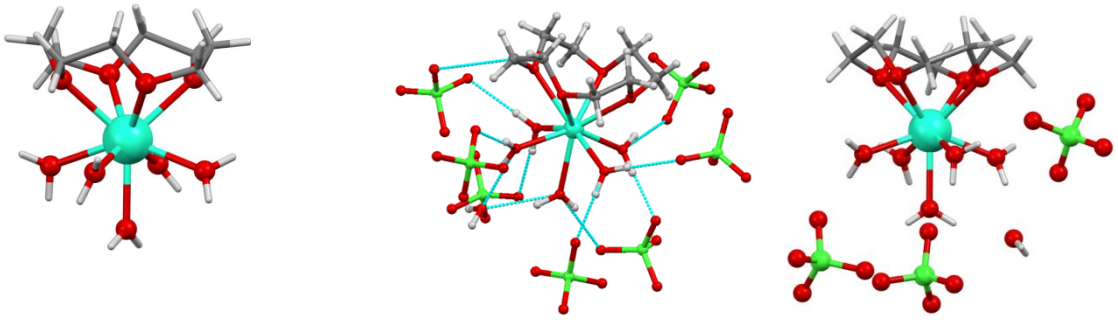

2A **2B** **2C**

Table 5.2 Energies of the first three lowest energy Kramers′ doublets for the three models of complexes **(1)** and **(2)** measured in cm^{-1}.

	1A	**1B**	**1C**	**2A**	**2B**	**2C**
$^6H_{\frac{15}{2}}$	0.000	0.000	0.00	0.000	0.000	0.000
	20.560	45.528	58.224	34.386	11.721	33.083
	59.050	77.849	68.724	67.185	77.170	66.942
	104.802	110.527	112.954	98.283	111.872	89.758
	146.372	180.244	177.132	137.295	141.467	131.235
	172.515	239.466	234.354	153.553	167.157	159.251
	236.856	276.889	268.554	211.099	216.841	198.393
	319.435	376.751	369.180	269.128	254.868	245.699
$^6H_{\frac{13}{2}}$	3013.524	3002.778	3525.412	3016.365	3525.534	3011.050
	3050.661	3067.240	3578.595	3048.317	3558.751	3049.813
	3080.949	3113.915	3627.942	3058.381	3582.730	3067.427
	3096.328	3134.278	3647.843	3063.738	3617.559	3091.087
	3135.303	3171.549	3680.367	3118.191	3643.377	3107.826
	3156.140	3189.595	3699.792	3145.341	3664.038	3129.249
	3205.383	3263.081	3776.225	3169.155	3675.308	3152.617
$^6H_{\frac{11}{2}}$	5575.344	5586.414	6071.999	5576.992	6058.959	5575.112
	5624.523	5637.116	6116.250	5617.031	6097.813	5617.497
	5656.378	5699.984	6175.548	5647.751	6130.629	5650.674
	5689.806	5726.415	6189.807	5684.009	6149.004	5671.289
	5740.490	5756.563	6215.591	5717.813	6194.988	5709.507
	5779.931	5835.245	6292.237	5751.463	6201.573	5733.642

Table 5.3 Main components of the *g*-tensors for the eight Kramers′ doublets of the $^6H_{15/2}$ level calculated with strong spin-orbit coupling for models **1A** – **1C** and **2A** – **2C**.

Doublet		1A	1B	1C	2A	2B	2C
1	g_x	0.809	0.599	0.258	0.617	0.535	0.903
	g_y	5.858	0.190	0.516	1.316	1.821	1.156
	g_z	13.131	17.727	17.492	18.190	17.808	17.819
2	g_x	1.522	0.201	0.835	0.539	0.575	1.189
	g_y	2.714	0.729	3.085	1.783	1.607	1.871
	g_z	13.384	17.301	15.442	16.314	16.639	16.377
3	g_x	8.824	10.261	0.000	3.601	3.621	8.115
	g_y	5.784	4.959	2.252	5.139	5.026	6.635
	g_z	1.877	2.439	9.949	10.402	10.714	3.002
4	g_x	1.982	1.522	9.133	1.708	10.743	0.486
	g_y	4.355	5.821	6.306	2.829	6.392	2.176
	g_z	10.132	8.527	3.036	14.332	0.295	14.629
5	g_x	9.021	0.730	0.708	0.912	10.881	1.515
	g_y	6.266	3.320	3.468	4.937	6.389	3.111
	g_z	2.874	12.314	11.625	11.328	1.522	10.822
6	g_x	0.219	0.329	0.330	11.379	3.047	10.089
	g_y	1.340	1.234	1.122	5.819	5.753	7.735
	g_z	16.586	17.749	17.521	0.046	9.023	0.391
7	g_x	1.668	1.125	1.285	2.268	1.829	7.600
	g_y	2.223	1.567	1.985	2.499	3.869	5.636
	g_z	16.001	16.293	15.943	12.527	6.157	3.587
8	g_x	0.286	0.214	0.182	0.528	1.137	0.817
	g_y	0.790	0.509	0.424	1.726	5.844	2.785
	g_z	18.669	18.774	18.781	17.426	14.342	16.888

From the data presented in Tables 5.2 and 5.3, it is clear that a consideration of species beyond the immediate coordination environment (i.e. hydrogen-bonded water molecules and perchlorate anions) of the chelated crown ether molecule must also be considered for an accurate representation of the electronic structure of the Dy^{III} centres within the crystal lattice. A complete analysis of the complexes was performed on models **1C** and **2C** which account for short-range electrostatic interactions between the positive dysprosium fragments and the surrounding molecules and perchlorate anions. These two models afford energy barriers that are in excellent agreement with the experimentally determined photoluminescence data. It should be noted that the theoretically calculated energy barrier for **(2)** is slightly larger than the experimentally

determined energy barriers, but this is consistent with the observations of Sessoli *et al.* for the Dy^{III} DOTA complex.[5,6]

Table 5.4 Angles (°) between the main magnetic axes (Z_m) of subsequent states for the full models of complex **(1)** and **(2)** (**1C** and **2C**, respectively) where 1 refers to the electronic ground state and 2, 3, 4 etc. refer to subsequent excited electronic states.

	1	**2**	**3**	**4**	**5**	**6**	**7**	**8**
Complex 1	---	55.5	54.0	32.4	114.2	56.3	65.0	66.2
Complex 2	---	72.5	86.7	95.3	77.1	106.3	21.5	122.1

S-6 Photoluminescence data

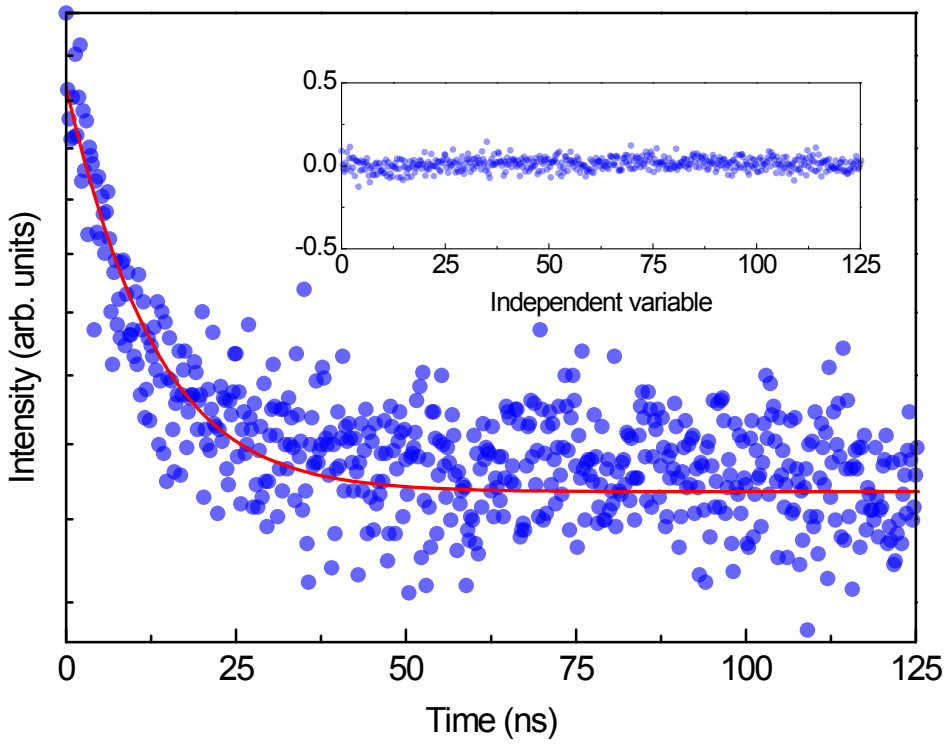

Figure 6.1. Emission decay curve of **1** excited at 390 nm and monitored at 480 nm. The straight line is the data best fit using a single exponential function. The inset shows the fit residual plot for a better judgment of the fit quality.

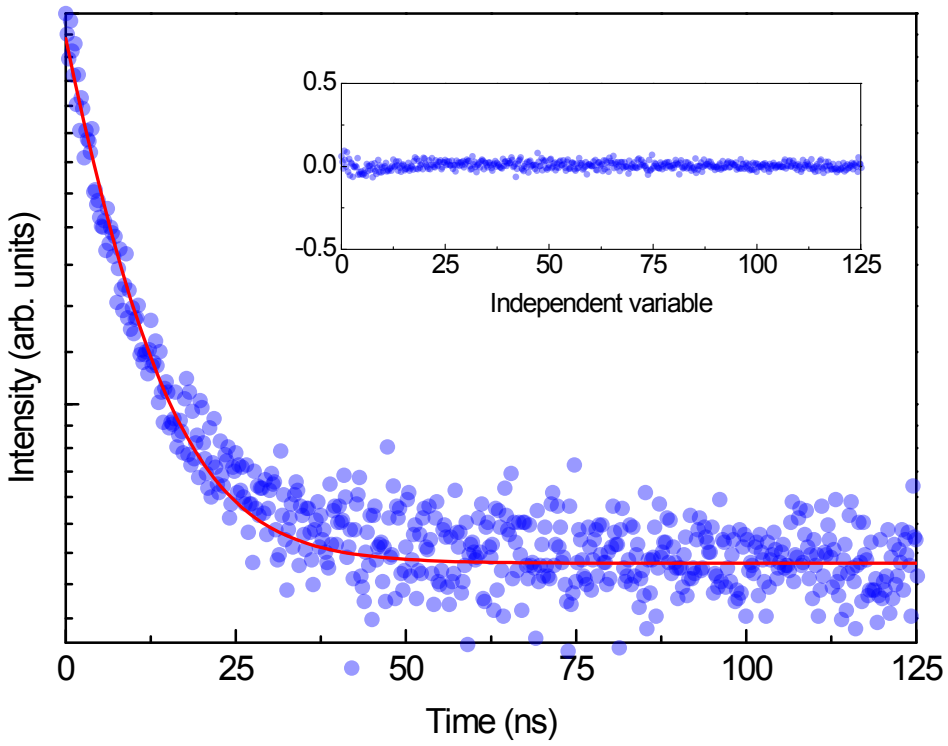

Figure 6.2. Emission decay curve of **2** excited at 390 nm and monitored at 480 nm. The straight line is the data best fit using a single exponential function. The inset shows the fit residual plot for a better judgment of the fit quality.

Figure 6.3. (A) High-resolution emission spectra (14 K) for **2** excited at 351 nm. (B) Magnification of the $^4F_{9/2} \rightarrow {}^6H_{15/2}$ transition and multi-Gaussian functions envelope fit (solid circles) and the components arising from the first $^4F_{9/2}$ Stark sublevel to the $^6H_{15/2}$ multiplet in the energy interval 20950-21100 cm^{-1}. (C) Regular residual plot (R^2~0.98) for a better judgment of the fit quality.

S-7 References

[1] H. Zabrodsky, S. Peleg and D. Avnir, D. *J.Am. Chem. Soc*., 1992, **114**, 7843.

[2] Y. -N. Guo, G.-F. Xu, Y. Guo and J. Tang, *Dalton Trans*., 2011, **40**, 9953.

[3] (a) F. Aquilante, L. De Vico, N. Ferré, G. Ghigo, P.-A, Malmqvist, P. Neogrády, T. B, Pedersen, M. Pitoňák, M. Reiher, B. O. Roos, L. Serrano-Andrés, M. Urban, V. Veryazov and R. Lindh, *J. Comp. Chem.* 2010, **31**, 224; (b) V. Veryazov, P.-O. Widmark, L. Serrano-Andrés, R. Lindh and B. O. Roos, *Int. J. Quant. Chem*., 2004, **100**, 626; (c) G. Karlström, R. L. Lindh, P.-A. Malmqvist, B.O. Roos, U. Ryde, V. Veryazov, P.O. Widmark, M. Cossi, B. Schimmelpfennig, P. Neogrady and L. Seijo, *Comp. Mater. Sci.*, 2003, **28**, 222.

[4] L. F. Chibotaru, L. Ungur and A. Soncini, *Angew. Chem. Int. Ed*., 2008, **47**, 4126.

[5] G. Cucinotta, M. Perfetti, J. Luzon, M. Etienne, P. E. Car, A, Caneschi, G. Calvez, K. Bernot and R. Sessoli, R. *Angew. Chem. Int. Ed*., 2012, **51**, 1606.